Journal of Applied Polymer Science

Novel Fabrication Route for Porous Silicon Carbide Ceramics Through the Combination of *In Situ* Polymerization and Reaction Bonding Techniques

Omid Ebrahimpour, Babak Esmaeili, Lucie Griffon, Jamal Chaouki, Charles Dubois
Department of Chemical Engineering, École Polytechnique de Montréal, P.O. Box 6079, Station Centre-Ville, Montréal, Canada
Correspondence to: C. Dubois (E-mail: charles.dubois@polymtl.ca)

ABSTRACT: For the first time, an *in situ* polymerization technique was applied to produce mullite-bonded porous SiC ceramics via a reaction bonding technique. In this study, SiC microsized particles and alumina nanopowders were successfully coated by polyethylene (PE), which was synthesized from the particle surface in a slurry phase reactor with a Ziegler–Natta catalyst system. The thermal studies of the resulting samples were performed with differential scanning calorimetry and thermogravimetric analysis. The morphology analysis obtained by transmission electron microscopy and scanning electron microscopy (SEM) confirmed that PE was successfully grafted onto the particle surface. Furthermore, the obtained porous ceramics were characterized in terms of their morphologies, phase composition, open porosity, pore size distribution, and mechanical strength. SEM observations and mercury porosimtery analysis revealed that the quality of the dispersion of nanosized alumina powder into the microsized SiC particles was strongly enhanced when the particles were coated by polymers with *in situ* polymerization. This resulted in a higher strength and porosity of the formed ceramic porous materials with respect to the traditional process. In addition, the X-ray diffraction results reveal that the amount of mullite as the binder increased significantly for the samples fabricated by this novel method. The effects of the sintering temperature, forming pressure, and polymer content on the physical and mechanical properties of the final porous ceramic were also evaluated in this study. © 2014 Wiley Periodicals, Inc. J. Appl. Polym. Sci. **2014**, *131*, 40425.

KEYWORDS: grafting; manufacturing; polyolefins; porous materials; properties and characterization

Received 28 October 2013; accepted 12 January 2014
DOI: 10.1002/app.40425

INTRODUCTION

Porous silicon carbide ceramics have attracted great interest in a broad range of high-temperature structural applications because of their superior physical properties, such as low thermal expansion coefficients, good thermal shock resistance, and excellent chemical and mechanical stabilities. They have been considered as potential candidate materials for high-temperature applications, such as hot-gas filters, membrane supports, refractory plates, and gas-burner media.[1,2] However, because of the strong covalent nature of the Si—C bond, which is due to its inherent structure, it is difficult to sinter SiC ceramics at a moderate temperature, and a high sintering temperature (>2000°C) is needed to self-bond SiC together.[3]

It has been reported that changing the sintering environment or adding secondary-phase bonded materials, such as alumina, enables the fabrication of porous SiC ceramics at lower sintering temperatures.[4] This process consists of the mixture of SiC particles with a sintering aid and a pore former in a suitable medium followed by drying, pressing, and finally, sintering in air instead of an inert atmosphere. Accordingly, fugitive agents burn out and form pore structures during the heating step. At higher temperatures, SiC particles partially oxidize to silica (SiO_2); then, they react with alumina (at >1400°C) to form mullite. Consequently, SiC particles are bonded by SiO_2 and mullite ($3Al_2O_3{\cdot}2SiO_2$) by means of *in situ* reaction bonding.[5] The fabricated mullite-bonded porous SiC ceramics are expected to have better physical and mechanical properties because of the good oxidation resistance of mullite and the similar thermal expansion coefficients between mullite and SiC.[6]

Being an attractive approach, this process has been investigated by various researchers to improve the final properties of the product. For example, the use of other additives such as Y_2O_3, CeO_2, and MgO to enhance the mechanical properties of porous SiC ceramics has been proposed.[6–9] Very recently, we studied the effect of the alumina content and sources (calcined alumina, alumina sol) on the mechanical and physical properties of porous ceramics. The results demonstrate that the addition of alumina nanopowder significantly increased the

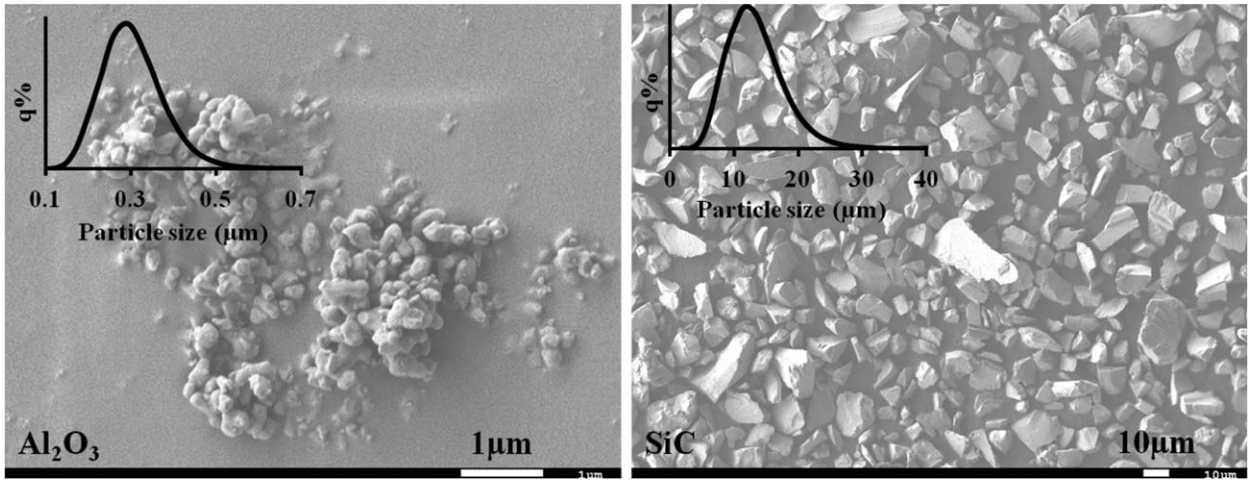

Figure 1. SEM micrographs and particle size distribution of the starting materials. q% = cumulative percentage.

mechanical strength and dramatically decreased the porosity.[10] To control the porosity of the final product, some pore formers, such as graphite, yeast, and polymer beads, have been used in the starting materials.[5,11,12]

Although considerable efforts have been devoted to improving the process, one of the main drawbacks of this method is the agglomeration of fine particles (sintering aids) because of the strong interactions between nanoparticles, which results in an insufficient dispersion of the starting particles during the preparation of the green body. For instance, it was reported that when alumina submicrometer particles were added to SiC microsized particles, most of them were agglomerated. As a result of the agglomeration, the alumina particles had only limited contact with the SiC micropowders and, therefore, could not fully participate in the mullite reaction.[5] Furthermore, this problem can severely impair the mechanical properties of the final ceramics. The dispersion of particles will be more problematic when different types of powders are used in the starting materials. For example, Ding et al.[5] used different particle sizes of graphite as pore formers in the starting materials. They observed a bimodal pore size distribution, which was attributed to the weak dispersion between the pore former and the starting materials. This agglomeration significantly decreased the constitutive properties of the product. Therefore, it is essential to develop an effective way to mitigate this problem and improve the material dispersion; this is the key aspect in the preparation of porous ceramics with excellent mechanical and physical properties.

To tackle this challenge, the modification of the surface of the initial materials by the growth of a polymer phase, which subsequently acts as a pore former, was proposed. This approach relies on an *in situ* polymerization process known as *grafting-from* rather than the physical mixing of the starting materials with the pore former. The preparation of inorganic or organic polymeric composites with enhanced properties is a well-known method.[13,14] Typically, in this technique, the monomer is polymerized from active compounds (initiators), which are covalently anchor on the surface of inorganic particles.[15,16] Monomers can penetrate easily through the aggregated nanoscale particles because of their inherent small size. As a result, synthesized polymer chains partially fill the free volume inside the nanoparticle aggregates, and therefore, the aggregated nanoparticles break out.[16] Hence, *in situ* polymerization is an attractive approach for the fabrication of porous ceramics with desired improved mechanical and physical properties.

This method has been applied successfully in the synthesis of composites materials for a broad range of inorganic particles, such as carbon nanotubes,[17] alumina,[18,19] SiO_2,[20–24] clay,[25–27] aluminum,[28] ZnO,[29] silver,[30] and silicon nitride,[31] with different polymerization routes. Similarly, our research group encapsulated zirconia nanoparticles with polyethylene (PE) via various techniques with a Ziegler–Natta catalyst.[32,33]

The main objective of this study was to investigate the implementation of *in situ* polymerization as a means of enhancing the dispersion of sintering additives into the starting materials to fabricate porous SiC ceramics with improved properties. We also aimed to adjust the porosity of the porous SiC ceramics by controlling the polymerization conditions and to manufacture porous SiC ceramics with improved mechanical and physical properties via a combination of the *in situ* polymerization and reaction bonding methods. To the best of our knowledge, this original work was accomplished by our group for the first time. We made a comparison between the traditional process and our developed method by investigating the flexural strength, open porosity, and pore size distribution of the final products. In addition, the effects of the polymer content, sintering temperature, and forming pressure on the phase composition and mechanical and physical properties of the final products were studied.

In this study, SiC microsized particles and alumina nanoparticles were primarily coated by PE via *in situ* polymerization in a benchtop batch reactor with a Ziegler–Natta catalyst system. After the materials were pressed to form a green body, they were placed in the furnace under air. During the heating cycle, the polymer was first removed by calcination; this created the desired porous morphology, and then at higher temperature, mullite was formed by a reaction between the oxidation-derived SiO_2 and alumina.

EXPERIMENTAL

Materials

Microsized α-SiC powder (99.7% purity, $\rho = 3.2$ g/cm^3, $S_{BET} = 0.87$ m^2/g; where ρ is density of the powders and S_{BET} is the specific surface area obtained by BET instrument) as the starting material and nanoparticle α-Al_2O_3 powder (99.95% purity, $\rho = 3.95$ g/cm^3, $S_{BET} = 8.5$ m^2/g) as the sintering additive were purchased from LABMAT (Canada). As shown in Figure 1, the SiC particles were irregular in shape and sharp at their edges compared to the alumina powders, which were more uniform. According to the particle size analysis, the volume-average mean particle size of SiC was determined to be 11.5 μm ($d_{10} = 6.6$ μm and $d_{90} = 16.2$ μm; the d_{90} is the diameter of powder where 90% of the distribution has a smaller particle size; and the d_{10} diameter has 10% smaller and 90% larger), and that of alumina was 270 nm ($d_{10} = 188$ nm and $d_{90} = 354$ nm). Ethylene gas (99.5% purity, Canadian Liquid Air) was used as the monomer for the polymerization reaction. The Ziegler–Natta catalyst system was constituted of titanium tetrachloride ($TiCl_4$, Fluka) as the catalyst with 1*M* triethylaluminum in hexane ($AlEt_3$, Sigma-Aldrich) as a cocatalyst. They were stored and handled in a glovebox under argon as they were highly sensitive to moisture and oxygen. Hexanes supplied by Sigma were dried and stored for at least 24 h on a molecular sieve and used as the reaction solvent.

In Situ Polymerization

The slurry polymerization experiments were performed in a 2-L pressurized BUCHI reactor heated with an external fluid bath circulator and equipped with a magnetic drive impeller. In a typical reaction, a mixture of SiC and alumina particles (18 g of SiC and 9.72 g of alumina, 35 wt % alumina), which was previously dried in an oven at the temperature of 150°C, was added to 1.5 L of dried hexane. The mixture was heated at the desired reaction temperature for about 1 h and continuously stirred in hexane by mechanical agitation (400 rpm). The system was then purged with N_2, which was dried further by passage through a molecular column sieve to eliminate oxygen in the medium. Subsequently, a predetermined amount of the catalyst, $TiCl_4$, was added with a syringe through a septum feeding port in the reactor. With a delay of 15 min after the first injection, the desired amount of cocatalyst $AlEt_3$ was also injected, and the mixture was agitated for another 5 min to ensure the formation of a catalyst–cocatalyst complex. The reaction was started by the initiation of a flow of ethylene monomer. For all of the experiments, the reaction temperature and the pressure were maintained constant at 65°C and 48 kPa, respectively. The amount of injected catalyst was determined on the basis of the total particle surface area of powders in the system, which could be ideally coated by $TiCl_4$ (7 mg of catalyst/g of powder). The molar ratio of the cocatalyst to catalyst was fixed at 2. After the desired reaction time, the polymerization was terminated by the injection of ethanol into the medium to hydrolyze the catalyst complex.

Fabrication of Porous SiC Ceramics

To manufacture the porous SiC ceramics, the polymer grafted particles were dried and passed through an 80-mesh screen. Afterward, they were pressed (at 25, 50, or 100 MPa) uniaxially into a rectangular bars with dimensions of 4.5 ×10.0 ×50.0 mm^3 with a stainless steel die. Subsequently, compact

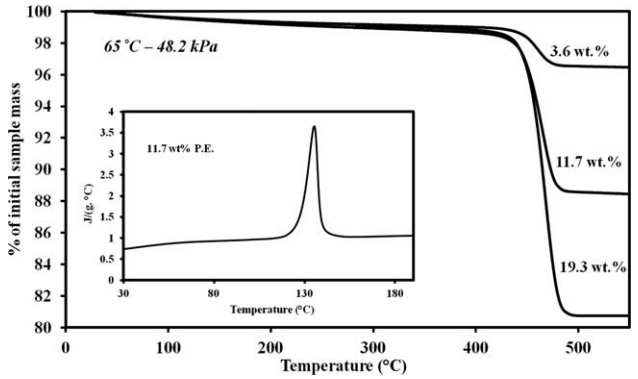

Figure 2. TGA of three PE-coated samples at different polymerization reaction times (4, 7, and 15 min). J = joule.

compounds were placed in a box furnace and heated up to 400°C at a heating rate of 2°C/min for 2 h to achieve polymer degradation. Subsequently, the temperature was increased up to 900°C at a heating rate of 2°C/min followed by a steeper ramp of 5°C/min to reach the desired sintering temperature (1500 or 1550°C). The samples were held at the sintering temperature for 3 h in air, and finally, the specimens were cooled down to room temperature at a cooling rate of 5°C/min.

Alternatively, to compare this developed process with the more traditional method, silicon carbide and submicrometer alumina powders with a weight ratio of 35 wt % were mixed with 2.5 wt % *poly(vinyl butyral)* as a binder in ethanol with a high-energy ball mill. After they were dried and passed through a screen, the powders were pressed and heated under air to produce porous samples. Further details about this part of the process were reported by our group elsewhere.[10]

Characterization

The mean particle size and the surface area of the starting powders were measured by a Horiba LA-950 laser diffraction particle size analyzer and a Quantachrome Autosorb-1 apparatus, respectively. Before Brunauer–Emmett–Teller analysis, the samples were degassed at 150°C for 3 h.

The quantity of polymer grafted from the particles was assessed by means of thermogravimetric analysis (TGA) with a TGA Q 5000 apparatus (TA Instruments) in a temperature range from 25 to 600°C at a heating rate of 10°C/min under a nitrogen atmosphere with a flow rate of 20 mL/min. The melting temperature and crystallization behavior of the synthesized polymer on the particles were studied by differential scanning calorimetry (DSC; DSC Q 2000, TA Instruments) at cooling and heating rates of 10°C/min. The morphological observation of the samples was conducted with scanning electron microscopy (SEM; model JSM-7600 TFE, JEOL, Japan) and by transmission electron microscopy (TEM; JEOL JEM-2100F) at a 200-kV acceleration voltage. The SEM was operated at 2 kV with LEI imaging mode and a working distance of 8.5 mm. X-ray diffraction (XRD) was performed with a Philips *X'Pert* diffractometer (The Netherlands) with Cu Kα radiation (0.154 nm) at a generator voltage of 50 kV and a current of 40 mA. The scanning rate was 1.2°/min at an interval of 0.02°. Furthermore, for the surface analysis, the coated samples and noncoated samples were

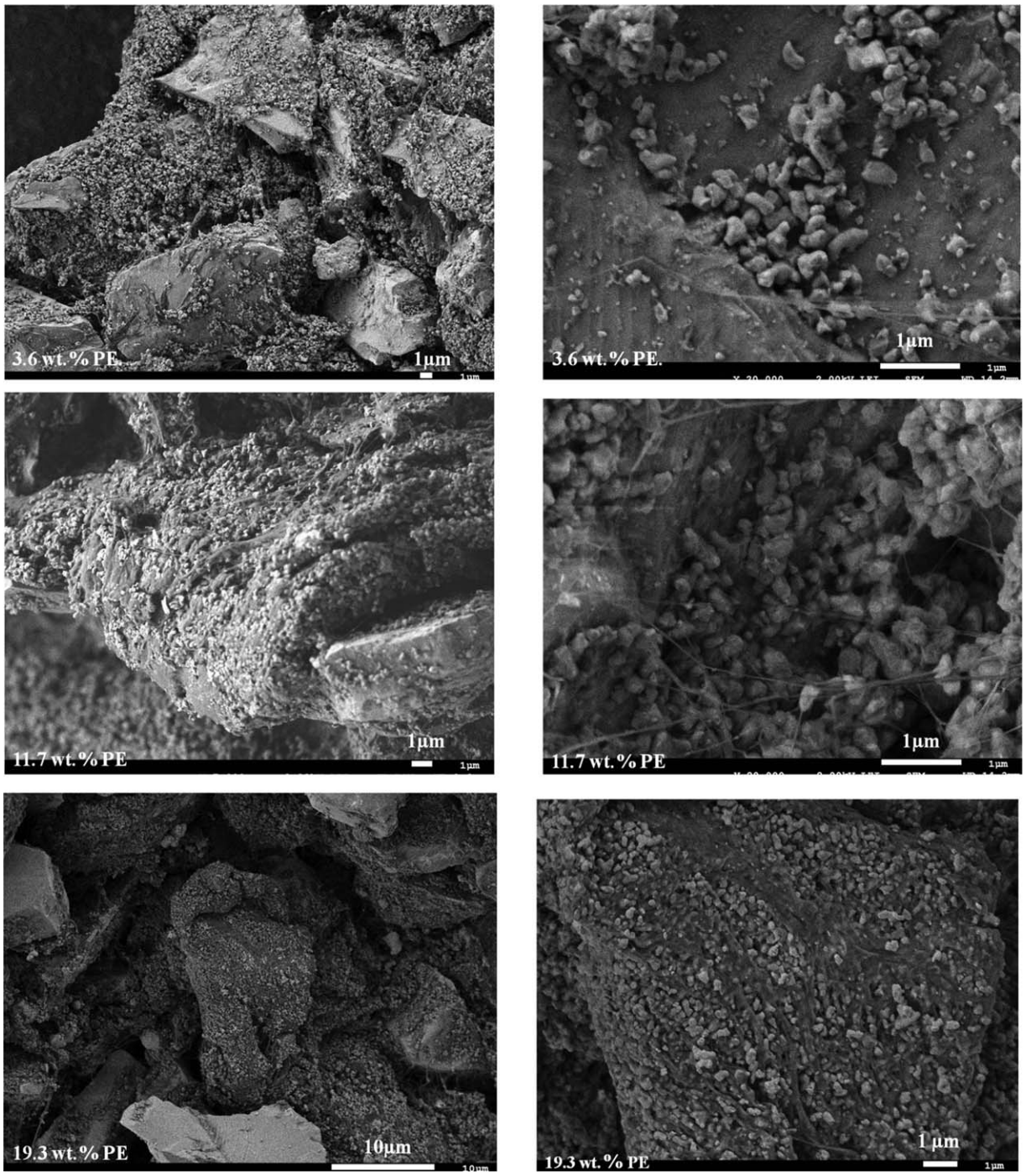

Figure 3. SEM images of coated SiC and Al_2O_3 particles with different amounts of the polymer.

analyzed by X-ray photoelectron spectroscopy (XPS) in a VG Scientific ESCALAB Mk II with Mg Kα radiation (1253.6 eV) operated at 300 W without a monochromator.

The true densities of the porous samples were measured by the *gas* volume displacement method with a gas pycnometer (Accupyc II 1330 helium pycnometer). Mercury porosimetry (Micromeritics Autopore IV) was used to show the pore size distribution of the porous samples. Open porosity was ascertained from the total mercury intrusion volume and the skeletal density of sample. The flexural strength of the porous samples was measured by a three-point bending test with a support distance of 30 mm and at a constant crosshead velocity of 0.5 mm/min with an Instron universal testing machine (model 1123, Instron, Canton, MA) with a 500-N load cell. The deflection measurement was taken with linear variable differential transformers (LVDT) with a resolution of 0.05%, and the Young's modulus was calculated via standard software (Instron Bluehill-2, UK). Beams were machined and polished to 3.0 ($\pm$0.1 mm) $\times$ 4.0 ($\pm$0.1 mm) $\times$ 36.0 mm,

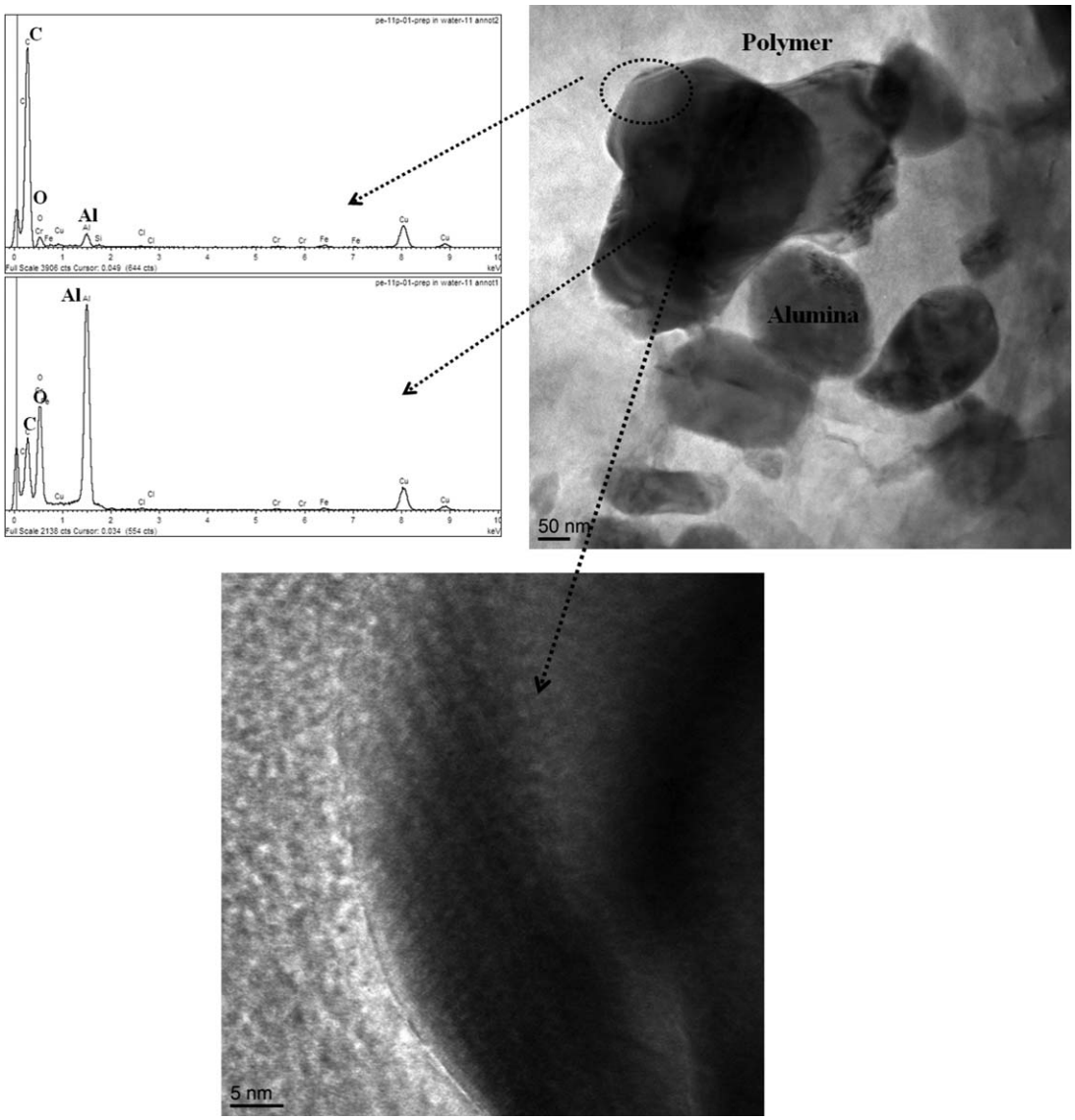

Figure 4. TEM images of the coated particles (11.7 wt % polymer).

and at least three specimens were tested to obtain the average strength.

RESULTS AND DISCUSSION

Characterization of the PE-Grafted SiC and Al_2O_3 Particles

The amount of polymer (pore formers) in the starting materials was determined by TGA tests. The TGA curves of the coated particles under an inert atmosphere at different polymerization reaction times (4, 7, and 15 min) are presented in Figure 2. As observed in the TGA curves, the weight loss occurred in two degradations steps. The first one between 150 and 350°C was associated with the pyrolysis of small oligomer chains. The major weight loss took place in the temperature range 425–485°C. It corresponded to the decomposition of high-molecular-weight PE to the olefinic and paraffinic components under nitrogen.[34–36] It should be noted that with increasing polymerization time, degradation appeared at a higher temperature; this indicated that longer polymer chains were produced.

The thermal behavior of the coated samples was investigated further by measurement of the melting temperature and the crystallinity of the synthesized polymers via DSC. To estimate the crystallinity of the high-density polyethylene (HDPE) component on the coated samples, a value of 293 J/g was used as the reference for the heat of fusion of 100% crystalline PE at the perfect crystalline melting point.[37] DSC scans (Figure 2) showed a single melting endotherm peak corresponding to the melting temperature of the PE. The typical melting temperature and degree of the crystallinity for the coating polymer (11.7 wt %) were 135.69°C and 61%, respectively; these values were in agreement with literature reports for the characteristic properties of HDPE.[38]

The SEM observations for the morphological study of the coated particles with different amounts of polymers are presented in Figure 3. We could clearly see that SiC and alumina particles were coated by the polymer. In addition, the presence of very thin filaments of polymer between the alumina

Table I. XPS Data for the Original and Coated Particles with 19.3 wt % Polymer

Name	Bonding energy (eV)	Atom %	
		Original	Coated
Al2p	75.7	21.4	2.7
Si2p	101.3	7.7	1.5
O1s	532.9	48.5	8.2
F1s	691.8	1.6	0.4
C1s	285.3	20.3	86.5
Ti2p	459.1	—	0.3
Cl2p	199.3	0.5	0.4

nanopowders and SiC micropowders was revealed. As SiC particles were too thick for the transmission electron microscopy (TEM) beam to go through, TEM analysis was only conducted on the alumina nanoparticles. Figure 4 shows the typical TEM–energy-dispersive X-ray spectroscopy (EDX) micrographs obtained for the coated particles with 11.7 wt % polymer. According to EDX analysis, the dark particles were assigned to the alumina nanoparticles, and the grayish white areas in Figure 4 represent the coating polymer. The carbon peak for the alumina particles (EDX analysis) showed the presence of the polymer on the surface of particles. It was clearly visible from TEM analysis that the alumina particles were surrounded and coated by the polymer, and a good interfacial adhesion between the PE and the particles existed. The high-resolution TEM image presented in Figure 4 indicates that HDPE formed a close interface with alumina; this implied a proper wetting between the matrix and particles. These observations by SEM and TEM provided strong evidence that PE was successfully grafted from the surface of the particles.

According to the literature, it was well established that there was a nanolayer of silica on the surface of silicon carbide. Siokou and Ntais[39] investigated the interaction between SiO_2 and $TiCl_4$ using XPS analysis, and they showed that the catalyst anchored onto the substrates surface through covalent bonding between Ti and hydroxyl groups on the particles.

As the surface of alumina and silica contain hydroxyl groups[40,41] it was proposed that $TiCl_4$ reacted with the surface hydroxyl groups on the substrate, as shown in the following reaction:[42,43]

$$x(-\mathrm{OH})+\mathrm{TiCl}_4 \rightarrow (-\mathrm{O})_x\mathrm{TiCl}_{4-x}+x(\mathrm{HCl}) \quad (1)$$

where $x=1$ for monofunctional compounds and $x=2$ for bifunctional compounds. As a result, the monomers were polymerized from the sample surface, and the polymer chains built up during the polymerization reaction.[44]

Table I compares the surface elemental analysis of the noncoated particles with 19.3 wt % coated particles as measured by XPS. The results show that the peak intensity and, therefore, the contribution of the Si, Al, and O elements decreased in the coated particles. On the other hand, the relative amount of carbon increased by about four times for the coated particles. It should be noted that even at a high amount of polymer, a few traces of Si and Al elements were detected by XPS analysis. One explanation was that the polymer thickness was less than 10 nm (which was in order of the elemental surface composition for the used XPS) in some parts of particles as found by TEM characterization (Figure 5). Also, this might have been due to the fact that the concentration of reactive sites on the particle surface was not great enough or was not uniform. It is worthwhile to point out that several parameters, such as the polymerization time, reaction temperature, pressure, and Al/Ti molar ratio, could influence the polymerization rate.[45] In addition, the reactivity of monomer strongly depended on its size. For example, ethylene was five times more reactive than propylene because of the lower size of ethylene in the polymerization with the Ziegler–Natta heterogeneous catalyst.

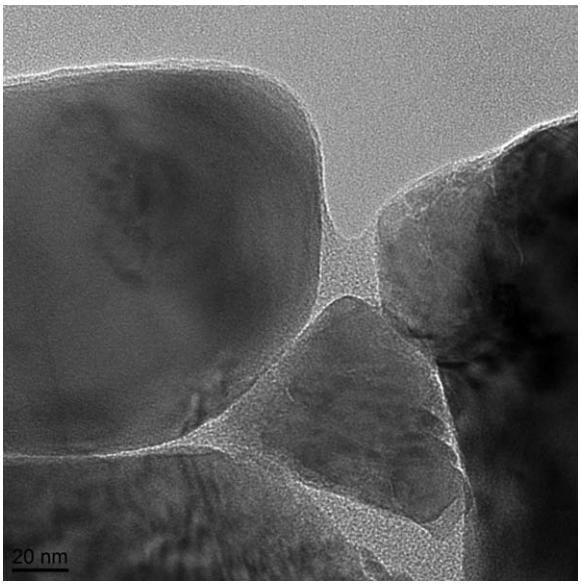

Figure 5. TEM micrograph of the coated particles with 11.7 wt % HDPE.

Characterization of the Porous SiC Ceramic Prepared by *In Situ* Polymerization

The skeletal density, flexural strength, open porosity, and average pore size of the porous SiC ceramic with different polymer contents are summarized in Table II. The samples were sintered at 1500°C for 3 h in air with a molding pressure of 50 MPa, where 35 wt % calcined alumina was added to the SiC particles. According to the results, we speculated that the introduction of the polymer via *in situ* polymerization on the particle surface could have been responsible for the increase in the flexural

Table II. Influence of the Polymer Content on the Flexural Strength, Open Porosity, and Pore Size

Polymer (w/w %)	Flexural strength (MPa)	Porosity (%)	Median pore diameter (μm)	Skeletal density (g/cm^3)
0	30.9 ± 1.3	32.3	1.57	3.11
3.6	50.1 ± 3.1	31.2	1.41	3.11
11.7	41.2 ± 1.7	36.8	1.90	3.12
19.3	28.1 ± 2.3	43.1	2.63	3.09

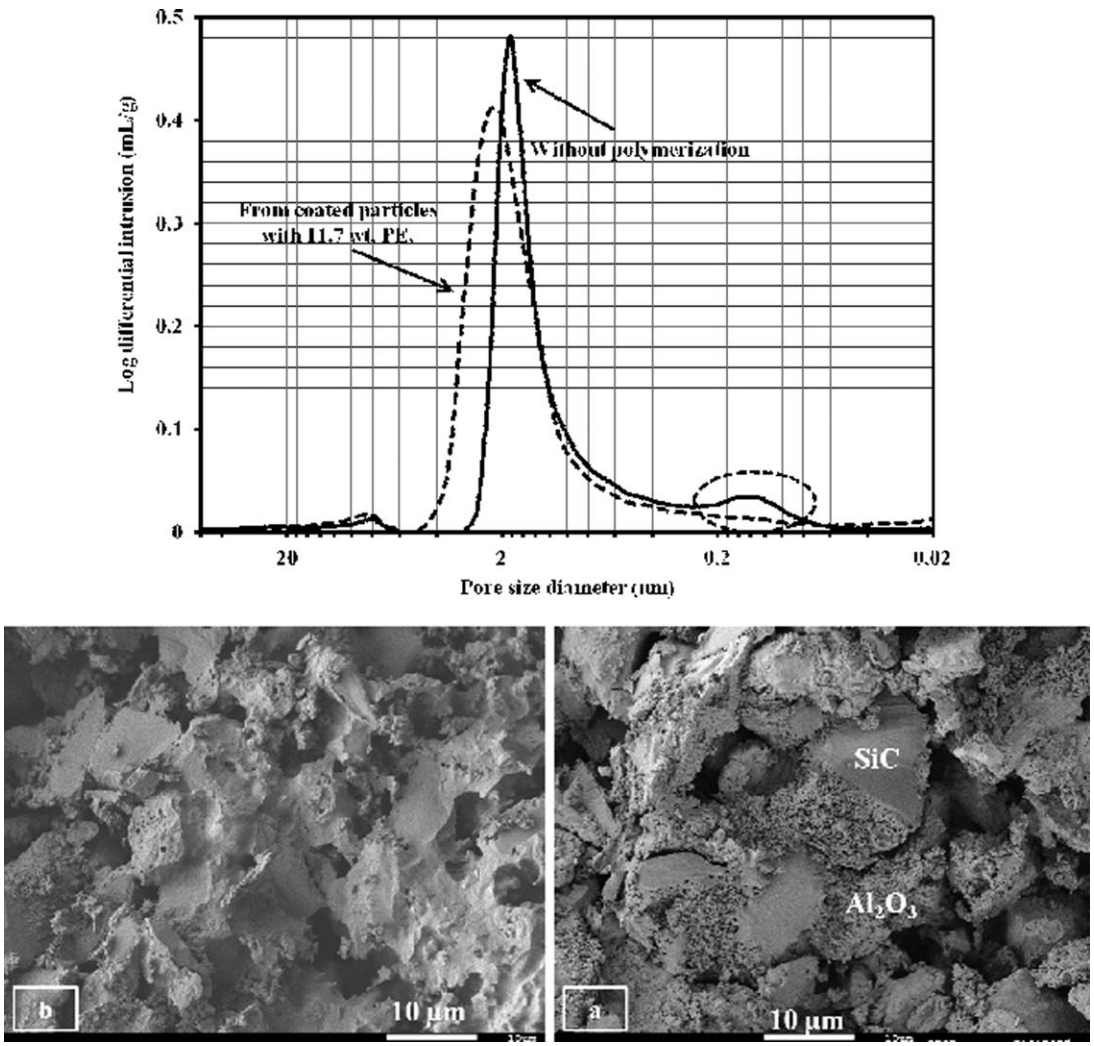

Figure 6. Pore size distribution and SEM images of the porous SiC ceramics sintered at 1500°C for 3 h in air, where 35 wt % calcined alumina was added to the SiC particles and where the starting particles were (a) not coated and (b) coated with 11.7 wt % PE.

strength compared to the conventional method, where the particles were simply mixed without any polymerization.

A typical pore size distribution and SEM morphology of the samples coated with 11.7 wt % polymer is compared with the one prepared without polymerization treatment in Figure 6. In the samples prepared with the conventional method, the pores were formed because of the stacking of SiC particles. As was clear in the SEM picture, some alumina particles were agglomerated and had no contact with SiC. The agglomeration produced some small pores, which caused another bump, as found in the pore size distribution results, whereas this agglomeration decreased remarkably in the case of the samples that were treated by *in situ* polymerization.

Figure 7 presents the XRD spectrum of the samples prepared with the traditional method and with the novel process at a sintering temperature of 1500°C for 3 h. For both methods, the phases consisted of mainly alumina, cristobalite, mullite, and silicon carbide. On the basis of the XRD pattern [Figure 7(a)], we concluded that when *in situ* polymerization was applied for the fabrication of the porous ceramic, the relative intensity of mullite to alumina increased as compared to the samples prepared by the conventional method.

According to the SEM observation and pore size distribution and XRD analysis, the enhancement of the physical and mechanical properties of the porous samples via the developed method can be explained as follows: when SiC and alumina nanosized powders were physically mixed in ethanol, a lot of alumina powders were agglomerated in the bulk system [Figure 8(a)], whereas for the samples that were introduced in polymerization, most of the nanoalumina powders were attached to the surface of the SiC powders [Figure 8(b)], and this led to the homogeneous dispersion of alumina particles. In fact, as a result of the deposition of the Ziegler–Natta catalyst on the SiC and alumina particles, the polymer chains grew from the particle surface. During the propagation of the polymer chains, they generated strong repulsion between the nanoparticles and eventually broke agglomerations between the aggregated alumina nanopowders. On the other hand, during the polymerization,

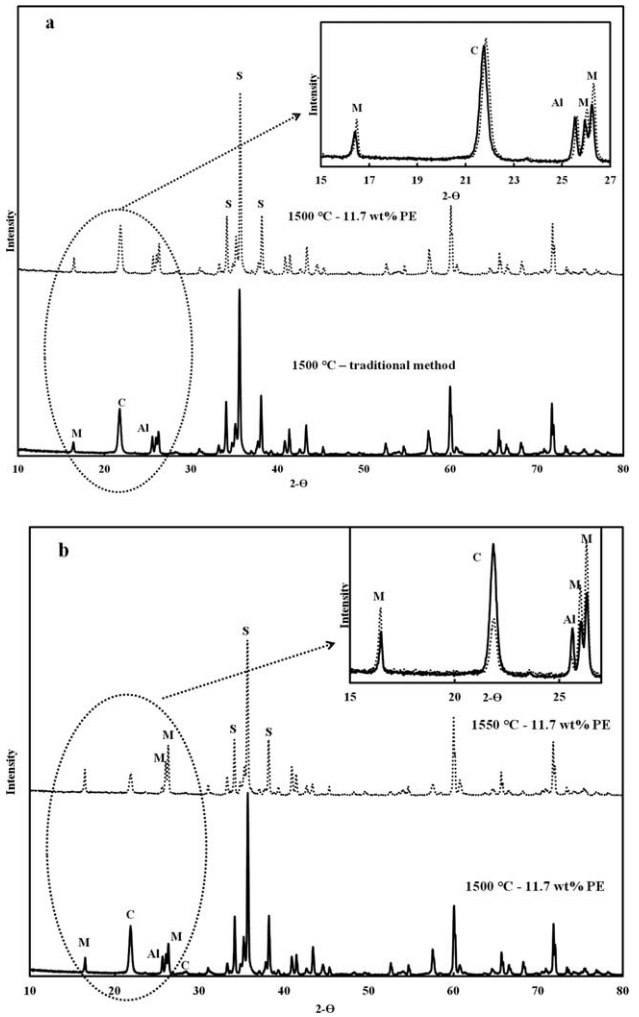

Figure 7. XRD patterns of the porous SiC ceramics: (a) effect of polymerization and (b) effect of the sintering temperature (Al = alumina, C = cristobalite, M = mullite, S = silicon carbide).

the polymer filaments attached and bonded alumina nanoparticles to the surface of the SiC particles; this provided a linkage between the alumina and SiC particles, as shown in Figure 9. In addition, because both particles (SiC and Al_2O_3) were coated by the polymer, their surface properties were similar; this facilitated the dispersion of powders in the solvent. Thus, during the formation of the green body, more alumina particles connected to the SiC particles, and they had more of a chance to react with the derived SiO_2 to form mullite than in the traditional method as found by XRD analysis. The SEM image [Figure 6(b)] clearly demonstrated better neck growth during the sintering of the samples as a result of more mullitization. Therefore, the increase in strength was ascribed to the better dispersion of alumina particles in SiC particles (Figure 6) and more mullite formation via *in situ* polymerization.

Typically, at a temperature above 800°C, SiC particles oxidized to silica via a passive oxidation reaction:

$$SiC + 2O_2 \rightarrow SiO_2(\text{amorphous}) + CO_2(g) \quad (2)$$

Previously, we reported that the oxidation rate of SiC strongly depended on the reaction temperature and SiC particle size.[46] The crystalline structure of silica was converted to the cristobalite phase when the temperature reached 1200°C:

$$SiO_2(\text{amorphous}) \rightarrow \text{Cristobalite} \quad (3)$$

At temperatures above 1400°C, alumina reacted with cristobalite to form mullite according to the following reaction:

$$3Al_2O_3 + 2SiO_2 \rightarrow 3Al_2O_3 \cdot 2SiO_2(\text{mullite}) \quad (4)$$

Figure 7(b) shows the effect of the sintering temperature on the evolution of the crystalline structure of samples that were prepared with 11.7 wt % polymer and sintered at 1500 and 1550°C for 3 h. The intensity of cristobalite and alumina decreased abruptly as a result of the extensive formation of mullite with increasing temperature. Another explanation for the decrease in the intensity of cristobalite was the formation of SiO gaseous. At lower sintering temperatures, oxidation occurred from the diffusion of oxygen into the surface of SiC, which formed a layer of silica film.[46] As the temperature increased, the surface of the SiC particles was covered by more mullite and silica, which acted as an oxidation barrier. Consequently, the partial pressure of oxygen decreased; this resulted in a change in the mechanism of

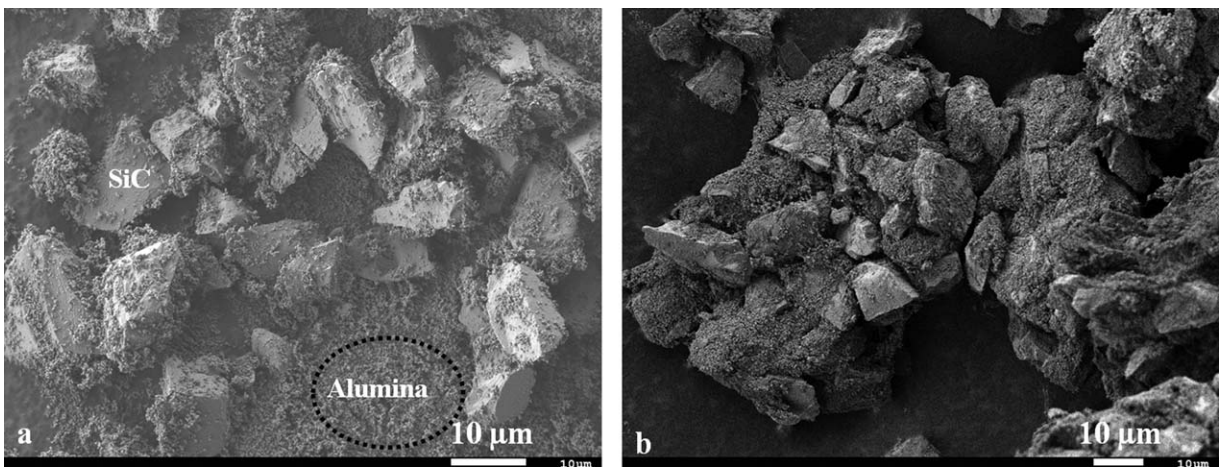

Figure 8. SEM micrographs of SiC and alumina (35 wt %) (a) mixed in ethanol and (b) coated by the polymer via *in situ* polymerization.

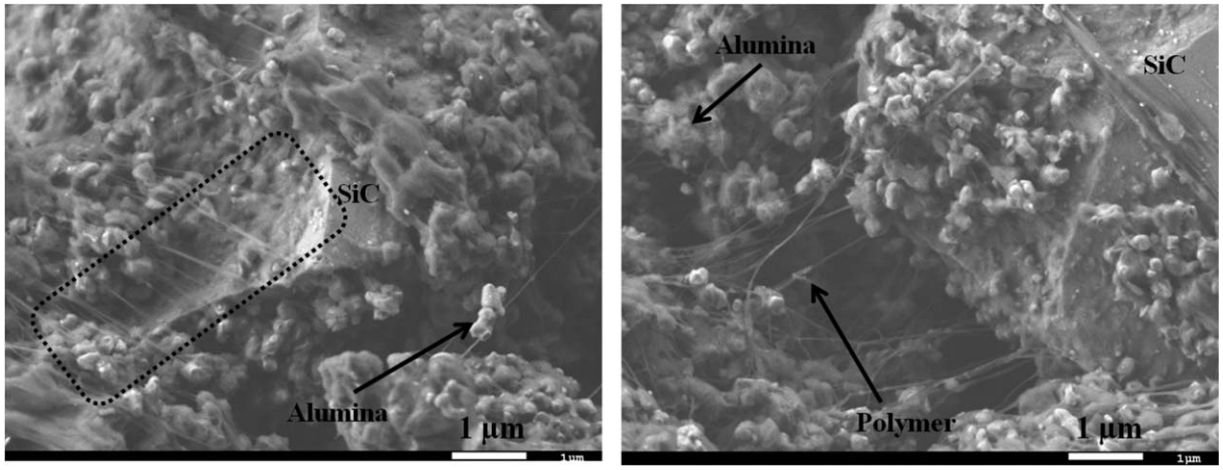

Figure 9. SEM micrographs of coated samples in which the polymer filaments attached alumina nanopowders on the SiC particles.

oxidation from the passive to active state, which produced gaseous SiO.

According to the literature, mullitization was controlled by the solution–precipitation mechanism.[47] At 1400°C, the nucleation of mullite occurred as a result of the penetration of fine α-Al_2O_3 particles into SiO_2, which acted like viscous softening. When the sintering temperature was increased to 1450°C, the viscosity of the SiO_2 glass decreased, and this enhanced the rate of diffusion of Al^{3+} ions into the viscous SiO_2 glass. When the sintering temperature was raised above 1500°C, the viscous flow promoted the rate of mullitization significantly by shortening the diffusion distances between SiO_2 and alumina. The SEM morphology (Figure 10) demonstrated the strong neck growth between the SiC particles and the formation of the needlelike mullite at a sintering temperature of 1550°C; this strongly supported the XRD results. After the formation of enough mullite, SiO_2 and α-Al_2O_3 must diffuse through the interfaces of SiO_2–mullite and Al_2O_3–mullite to conduct a further reaction.[48] Therefore, the mechanism of mullitization was diffusion-controlled. Increasing the sintering temperature also led to the filling of some small pores by the liquid phase and, consequently, a decrease in the sample porosity from 37.3 to 34.5%. For this case, the strength was enhanced from 41.2 to 51 MPa when the sintering temperature was increased from 1500 to 1550°C.

The results in Table II indicate that the sample porosity increased substantially when the polymer content changed from 31.2% to 43.1%, whereas the flexural strength decreased. The highest value of the mechanical strength was found to be about 50 MPa when the particles were coated with a low amount of polymer. The effect of the polymer content on the morphologies and pore size distribution of the porous SiC ceramics are presented in Figure 11. Accordingly, we found that with increasing polymer content, larger pores were created in the final product. The SEM images in Figure 11 show the microstructure of the fracture surfaces in the specimens with different amounts of polymer (3.6 and 19.3 wt %). We observed that in the sample with a lower amount of polymer, more SiC particles were connected, and larger growth necks between the SiC particles were observed. This enhanced the mechanical strength of the produced samples.

The relationship between the strength of a porous material and the porosity can be expressed by the following equation proposed by Rice:[49]

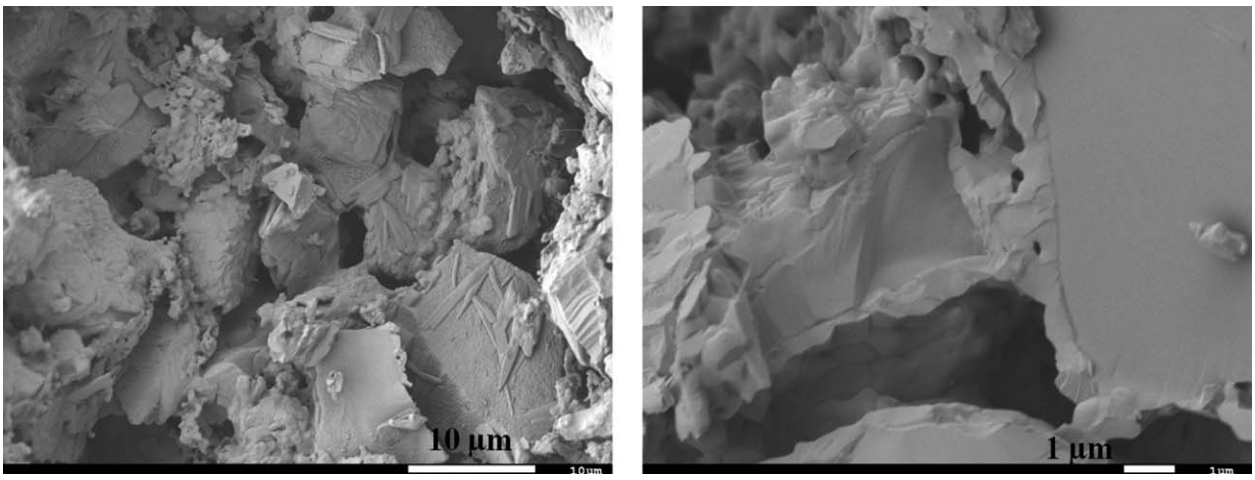

Figure 10. SEM of the porous SiC ceramics sintered at 1550°C for 3 h in air where 35 wt % calcined alumina was added to the SiC particles and they were coated with 11.7 wt % PE.

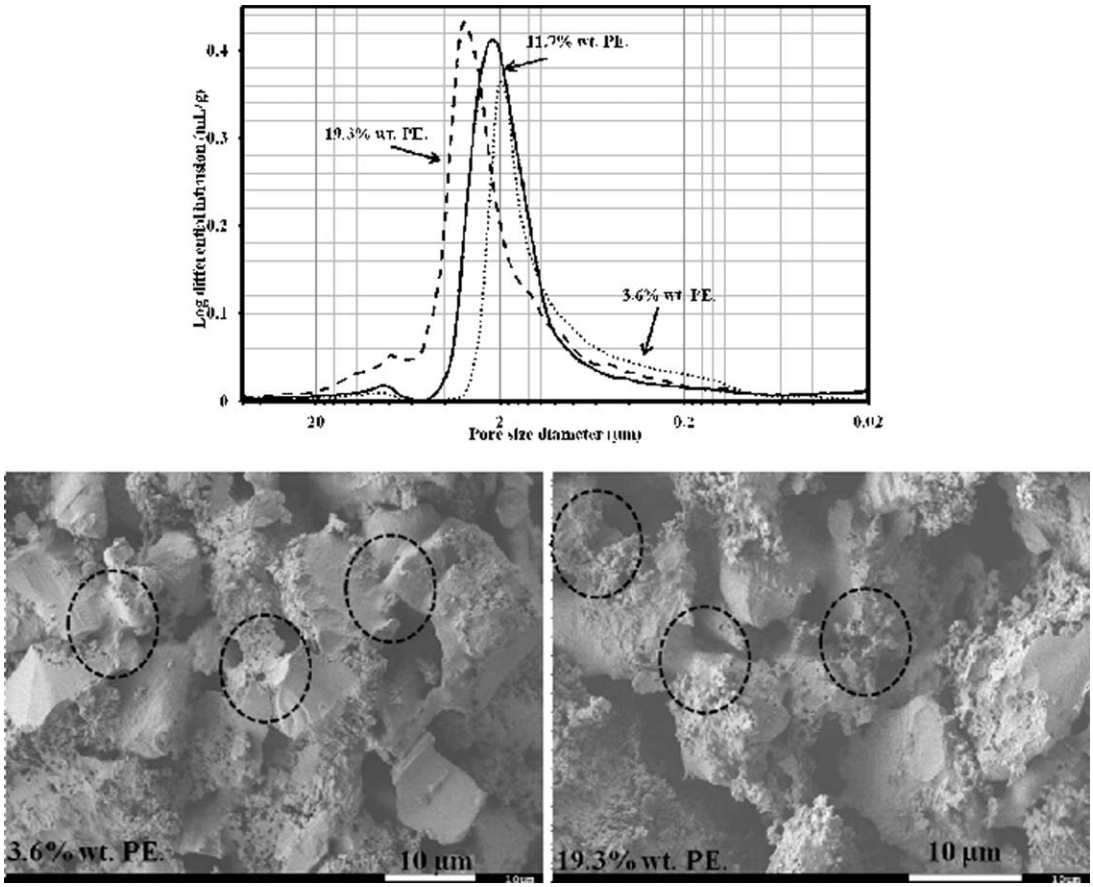

Figure 11. Pore size distribution and SEM of the porous SiC ceramics sintered at 1500°C for 3 h in air, where 35 wt % calcined alumina was added to the SiC particles and where the starting particles were coated with different amounts of PE.

$$\sigma = \sigma_0 \exp(-bP) \quad (5)$$

where σ_0 and σ are the strengths of the nonporous structure and the porous material at a porosity P, respectively, and b is an empirical constant that depends on the pore structure and material composition. The parameters of σ_0 and b were obtained to be 235.1 MPa and 4.9, respectively, by the fitting of the resulting samples with different polymer contents with linear regression ($R^2 = 0.977$). We noticed that the σ_0 and b parameters depended strongly on the processing conditions. For example, She et al.[4] reported values of $\sigma_0 = 190$ MPa and $b = 4.36$ for mullite-boned porous SiC ceramics, whereas Chun and Kim[50] reported a value of $b = 7.95$ for silica-bonded porous SiC ceramics.

Table III contains the physical and mechanical properties of porous samples as a function of the forming pressure where 3.6 wt % polymer was initially used and the specimens were later sintered at 1500°C for 3 h. The results show that in contrast to the polymer content, the compaction pressure had a direct effect on the strength. With increasing forming pressure from 25 to 100 MPa, the mechanical strength increased by about 100%, whereas the porosity and median pore diameter shifted to smaller values. XRD pattern analysis (the results are not shown) revealed that at a higher forming pressure, the relative intensity of mullite to alumina increased slightly. Increasing the forming pressure reduced the space between particles and the porosity, as shown in Figure 12. Therefore, the diffusion of α-Al_2O_3 through silica particles sped up, and the mullitization rate increased. Consequently, the flexural strength of the porous SiC ceramics improved as a result of well-developed necks between the SiC particles.

According to the experimental results presented in this article, we confirmed that the introduction of a polymer layer to the starting materials by *in situ* polymerization was a versatile method for producing porous ceramics with a higher strength and porosity compared to the traditional method. Another main advantage of the implementation of *in situ* polymerization for this application is that it resolves the problem of the holding, transferring, and even machining of the ceramic porous

Table III. Effect of the Forming Pressure on the Flexural Strength, Open Porosity, and Pore Size

Forming pressure (MPa)	Flexural strength (MPa)	Porosity (%)	Median pore diameter (μm)	Skeletal density (g/cm^3)
25	32.8 ± 3.4	38.3	2.19	3.12
50	50.1 ± 3.1	31.2	1.41	3.11
100	64.4 ± 8.4	27.1	1.18	3.10

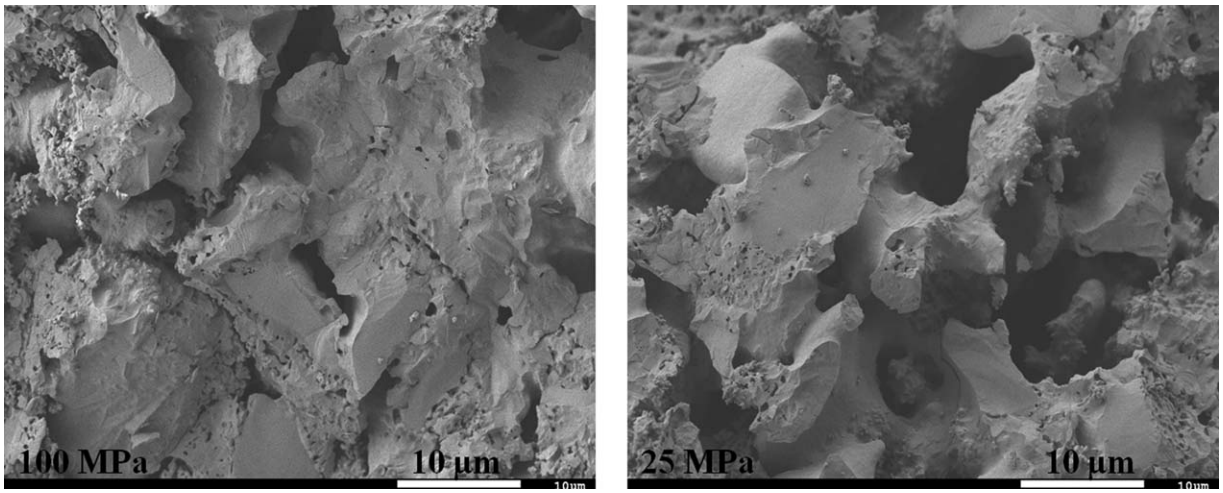

Figure 12. SEM morphologies of the porous SiC ceramics sintered at 1500°C for 3 h in air with a formation pressures of green bodies of 25 and 100 MPa, where 35 wt % alumina was added to the SiC particles and the starting particles were coated with 3.6 wt % polymer.

before firing. We noticed that the green product formed by this technique exhibited a higher strength stability; this made them much safer for handling and machining in comparison with those formed by the traditional method. This enhancement was attributed to the strong filler–matrix interfacial adhesion during the green body formation because the polymer provided better bonding between the SiC and alumina. The polymerization efficiency was improved when the particle surface was pretreated to increase the number of hydroxyl groups on the material surface with which the catalyst could react. For example, the modification of the SiC particles and alumina nanosize powders with alumina sol before polymerization may be an efficient way to increase the adhesion between the matrix and the particles. This hypothesis will soon be evaluated in a future and more thorough investigation.

CONCLUSIONS

In this study, a new process was developed to produce porous SiC ceramics with a combination of *in situ* polymerization and *in situ* reaction bonding techniques. SiC particles as the starting materials and alumina nanoparticles as the sintering additives were successfully coated by PE through an *in situ* polymerization process, in which the $TiCl_4$ catalyst was initially anchored covalently on the particle surface to subsequently initiate the polymerization of ethylene from the surface of the particles. TGA showed that HDPE was synthesized at different reaction times, and SEM and TEM observations provided direct evidence for the formation of macromolecular chains on the particles.

A comparison of the produced porous ceramics via a novel route with the ones obtained from the more traditional method revealed that both the mechanical and physical properties of the resulting products were significantly improved. XRD and SEM analysis confirmed that the SiC particles were bonded by both mullite and cristobalite. The pore size distribution analysis of the samples showed that the coating of the particles with the polymer via *in situ* polymerization induced an appropriate dispersion of nanopowders into the micro-SiC particles and led to a better homogeneity of the final product. As a result of the better dispersion and connection of alumina to SiC particles by the polymer chains, more mullite was produced because of the reaction between the alumina and SiO_2, as observed by XRD examination.

Moreover, we found that increases in the sintering temperature and the forming pressure had significant effects on the strength and porosity of the porous materials. In contrast, increases in the polymer content caused less contact between the SiC particles; this led to weak neck growth, increased porosity, and decreased mechanical strength of the ceramic porous materials. In this study, we measured flexural strengths between 28 to 64 MPa in conjunction with samples ranging from 43 to 27% in porosity by controlling the process conditions, such as the forming pressure and polymer content.

ACKNOWLEDGMENTS

This research was financially supported by Natural Sciences and Engineering Research Council of Canada (NSERC) through an Idea to Innovation grant. The authors acknowledge Sylvie St-Amour (FPInnovations, Canada) for her assistance with the mercury porosimetry measurements and Robert Delisle (Chemical Engineering Department, Polytechnique Montreal) for his technical support regarding the experimental setup.

REFERENCES

1. Kennedy, G. P.; Lim, K. Y.; Kim, Y. W.; Song, I. H.; Kim, H. D. *Met. Mater. Int.* **2011**, *17*, 599.
2. Liu, S. F.; Zeng, Y. P.; Jiang, D. L. *Int. J. Appl. Ceram. Technol.* **2009**, *6*, 617.
3. Sigl, L. S.; Kleebe, H. J. *J. Am. Ceram. Soc.* **1993**, *76*, 773.
4. She, J. H.; Deng, Z. Y.; Daniel-Doni, J.; Ohji, T. *J. Mater. Sci.* **2002**, *37*, 3615.
5. Ding, S. Q.; Zhu, S. M.; Zeng, Y. P.; Jiang, D. L. *J. Eur. Ceram. Soc.* **2007**, *27*, 2095.

6. Liu, S. F.; Zeng, Y. P.; Jiang, D. L. *J. Eur. Ceram. Soc.* **2009**, *29*, 1795.
7. Ding, S. Q.; Zhu, S. M.; Zeng, Y. P.; Jiang, D. L. *Ceram. Int.* **2006**, *32*, 461.
8. Choi, Y. H.; Kim, Y. W.; Han, I. S.; Woo, S. K. *J. Mater. Sci.* **2010**, *45*, 6841.
9. Eom, J. H.; Kim, Y. W. *J. Mater. Sci.* **2009**, *44*, 4482.
10. Ebrahimpour, O.; Dubois, C.; Chaouki, J. *J. Eur. Ceram. Soc.* **2014**, *34*, 237.
11. Chi, W. G.; Jiang, D. L.; Huang, Z. R.; Tan, S. H. *Ceram. Int.* **2004**, *30*, 869.
12. Chun, Y. S.; Kim, Y. W. *Met. Mater. Int.* **2005**, *11*, 351.
13. Rajabian, M.; Dubois, C. *Polym. Compos.* **2006**, *27*, 129.
14. Caruso, F. *Adv. Mater.* **2001**, *13*, 11.
15. Esmaeili, B.; Dubois, C.; Carreau, P. J.; Heuzey, M. C. *Int. Polym. Proc.* **2013**, *28*, 331.
16. Kango, S.; Kalia, S.; Celli, A.; Njuguna, J.; Habibi, Y.; Kumar, R. *Prog. Polym. Sci.* **2013**, *38*, 1232.
17. Trujillo, M.; Arnal, M. L.; Muller, A. J.; Laredo, E.; Bredeau, S.; Bonduel, D.; Dubois, P. *Macromolecules* **2007**, *40*, 6268.
18. Zhang, X.; Simon, L. C. *Macromol. Mater. Eng.* **2005**, *290*, 573.
19. Cinausero, N.; Azema, N.; Cuesta, J. M. L.; Cochez, M.; Ferriol, M. *Polym. Adv. Technol.* **2011**, *22*, 1931.
20. Zou, H.; Wu, S. S.; Shen, J. *Chem. Rev.* **2008**, *108*, 3893.
21. Liu, G. Y.; Li, L. Y.; Yang, X. L.; Dai, Z. *Polym. Adv. Technol.* **2008**, *19*, 1922.
22. Dubois, C.; Rajabian, M.; Rodrigue, D. *Polym. Eng. Sci.* **2006**, *46*, 360.
23. Zapata, P.; Quijada, R.; Benavente, R. *J. Appl. Polym. Sci.* **2011**, *119*, 1771.
24. Azinfar, B.; Ahmad Ramazani, S. A.; Jafariesfad, N. *Polym. Compos.* **2014**, *35*, 37.
25. Nikkhah, S. J.; Ramazani, A.; Baniasadi, H.; Tavakolzadeh, F. *Mater. Des.* **2009**, *30*, 2309.
26. Ma, J. S.; Qi, Z. N.; Hu, Y. L. *J. Appl. Polym. Sci.* **2001**, *82*, 3611.
27. Zapata, P.; Quijada, R.; Covarrubias, C.; Moncada, E.; Retuert, J. *J. Appl. Polym. Sci.* **2009**, *113*, 2368.
28. Esmaeili, B.; Chaouki, J.; Dubois, C. *Polym. Eng. Sci.* **2012**, *52*, 637.
29. Hong, R. Y.; Qian, J. Z.; Cao, J. X. *Powder Technol.* **2006**, *163*, 160.
30. Zapata, P. A.; Tamayo, L.; Páez, M.; Cerda, E.; Azócar, I.; Rabagliati, F. M. *Eur. Polym. J.* **2011**, *47*, 1541.
31. Sohail, O. B.; Jabarullah Khan, M.; Sreekumar, P. A.; Al-Harthi, M. A. *Polym. Eng. Sci* **2013**. DOI: 10.1002/pen.23744.
32. Esmaeili, B.; Chaouki, J.; Dubois, C. *AIChE J.* **2009**, *55*, 2271.
33. Esmaeili, B.; Chaouki, J.; Dubois, C. *Macromol. Symp.* **2006**, *243*, 268.
34. Peterson, J. D.; Vyazovkin, S.; Wight, C. A. *Macromol. Chem. Phys.* **2001**, *202*, 775.
35. Marongiu, A.; Faravelli, T.; Ranzi, E. *J. Anal. Appl. Pyrol.* **2007**, *78*, 343.
36. Chrissafis, K.; Paraskevopoulos, K. M.; Pavlidou, E.; Bikiaris, D. *Thermochim. Acta* **2009**, *485*, 65.
37. Rachtanapun, P.; Selke, S. E. M.; Matuana, L. M. *J. Appl. Polym. Sci.* **2003**, *88*, 2842.
38. Osman, M. A.; Atallah, A. *Macromol. Rapid Commun.* **2004**, *25*, 1540.
39. Siokou, A.; Ntais, S. *Surf. Sci.* **2003**, *540*, 379.
40. McCafferty, E.; Wightman, J. P. *Surf. Interface Anal.* **1998**, *26*, 549.
41. Ma, G.; Liu, D. F.; Allen, H. C. *Langmuir* **2004**, *20*, 11620.
42. Wang, Q.; Kaliaguine, S.; Aitkadi, A. *J. Appl. Polym. Sci.* **1992**, *44*, 1107.
43. Jin, Y. H.; Park, H. J.; Im, S. S.; Kwak, S. Y.; Kwak, S. *Macromol. Rapid Commun.* **2002**, *23*, 135.
44. Siokou, A.; Ntais, S. *Surf. Sci.* **2003**, *540*, 379.
45. Ramazani, S. A. A.; Tavakolzadeh, F.; Baniasadi, H. *J. Appl. Polym. Sci.* **2010**, *115*, 308.
46. Ebrahimpour, O.; Chaouki, J.; Dubois, C. *J. Mater. Sci.* **2013**, *48*, 4396.
47. Davis, R. F.; Pask, J. A. *J. Am. Ceram. Soc.* **1972**, *55*, 525.
48. Saruhan, B.; Albers, W.; Schneider, H.; Kaysser, W. A. *J. Eur. Ceram. Soc.* **1996**, *16*, 1075.
49. Rice, R. W. *J. Mater. Sci.* **1993**, *28*, 2187.
50. Chun, Y.-S.; Kim, Y.-W. *Met. Mater. Int.* **2005**, *11*, 351.